ORIGINAL PAPER

Pore Size Distributions and Multi-Fractal Characteristics of the Intact and Pulverized Coal in High Gas Mine

Jie Zhu [ORCID] · **Yuhang Yang · Tangsha Shao · Chenyu Hou · Yaodong Jiang · Yuhan Zhao · Jinge Wang · Jiazhi Li**

Abstract The pore structure and microfracture evolution characteristics of coal in high gas mine are worthy of studying to make clear the mechanism of coal and gas outburst. Samples were collected from 2# coal seam (high gas coal seam) in Dongpang Coal Mine, China. Two groups of samples were divided: one was cut from the intact coal blocks which was roughly a cube with the particle size less than 1 cm, and the other was the pulverized coal drilled from the working face. Mercury intrusion porosimetry (MIP) and gas absorption were used to investigate the pore size distributions (PSDs) of coal samples. The experimental results display that the compressibility of coal matrix has a significant influence on the pore volume of coal specimens especially when the pressure is greater than 20 MPa. Macropores in both intact and pulverized coal samples account for the largest proportion but the average micropore volume for the pulverized coal is 2.67 times that of the intact coal. The greater pore tortuosity of pulverized coal indicates that it has worse pore connectivity overall. Multi-fractal analysis result shows the PSDs of pulverized coal are more homogeneous than intact coal. During the process of mining, the vertical loading and horizontal unloading cause the opening and propagation of microfractures and increase the difference of the PSDs between the intact and pulverized coal. It results in the not smooth of gas flow from pulverized coal area. Gas might be prone to accumulate in the area with more pulverized coal.

Keywords Pore size distributions · Multi-fractal characters · High gas mine · Mercury intrusion porosimetry · Microfractures

1 Introduction

Coal and gas outburst is a phenomenon of sudden ejection of gas and coal rocks from the coal face within a short time (Li et al. 2003). The commonly accepted hypothesis of gas outburst holds that gas outburst is the result of the multiple actions, such as ground stress, the physical and mechanical properties of gas and coal. Among them, broken coal is an important factor for gas outburst (Beamish and Crosdale 1998; Cheng and Lei 2021). It is shown that a large amount of pulverized coal also appears at the scene of gas outburst. Different particle sizes of coal has a noticeable effect on its physico-mechanical properties and characteristics of coal–gas outburst (Guo et al. 2018; Zhuo et al. 2020). It is generally believed that the reduction of coal particle size mainly increases the porosity and total pore volume of coal (Xu et al. 2010; Guo et al. 2014). Therefore, in order to give the early warning of coal and gas

J. Zhu (✉) · Y. Yang · T. Shao · C. Hou · Y. Jiang · Y. Zhao · J. Wang · J. Li
School of Mechanics and Civil Engineering, China University of Mining and Technology (Beijing), Beijing 100083, China
e-mail: zhujie@cumtb.edu.cn

outburst, attention should be paid to the differences between intact coal and pulverized coal regions and its influence on gas diffusion and flow (Jin et al. 2016; Wang et al. 2019).

Many methods are used to study the pore characteristics of porous materials. The indirect methods include mercury intrusion porosimetry (MIP) (Li et al. 1999), gas adsorption (Cai et al. 2013), and nuclear magnetic resonance (NMR) (Suggate and Dickinson 2004), etc., which can obtain the pore size distributions (PSDs) of porous media. The direct measurements can observe the size and morphology of pore obviously, such as scanning electron microscopy (SEM) (Giffin et al. 2013) and X-ray CT imaging (Karacan and Okandan 2001). The pores with pore size above 3 nm can be measured by MIP. But when the intrusion pressure is greater than a certain value, the pressure may damage certain pores and the compressibility of coal matrix maybe replace pore filling (Friesen and Mikula 1988; Li et al. 1999). Therefore, Low-temperature nitrogen gas adsorption (LNA) which can investigate pore characteristic in the range of 1.7 nm to 271.3 nm and low-temperature carbon dioxide adsorption (LCA) that is employed to describe the microporosity with pore size less than 2 nm are used to correct the characterization of the PSDs by MIP. Based on Hg porosimetry and Fick's first law that can describe the fluid diffusion, pore tortuosity τ in porous solids is also deduced from their properties of the connected porosity (Carniglia 1986).

However, the randomness of pore spatial distributions makes it difficult to characterize its complexity mathematically for traditional Euclidean geometry (Li et al. 2015). The fractal theories originally proposed by Mandelbrot (1967), have been applied to quantitatively describe the physical properties of spatial inhomogeneity. The fractal dimension represents the internal irregular distributions of pores for porous media (Fu et al. 2001; Gauden et al. 2001). The heterogeneous PSDs of coal also can be discovered by multi-fractal analysis (Muller and McCauley 1992; Caniego et al. 2003). By investigating the local densities of pore and fracture distributions, multi-fractal analysis can describe them by fractal dimensions spectrum such as singularity dimension spectrum and generalized dimension spectrum (Chhabra et al. 1989; Ferreiro and Vázquez 2010). Multi-fractal approach provides a "fingerprint" to distinguish the effect of coal compression from the pore filling

process during mercury intrusion (Li et al. 1999) and is also appropriate to distinguish the PSDs of tectonically deformed coals (TDCs) in detail (Li et al. 2015).

In this paper, intact and pulverized coal from No.20011 working face of 2# coal seam (high gas coal seam) in the Dongpang Mine were applied to study the influence of coal matrix compressibility and obtain the comprehensive characteristics of the PSDs by MIP, LNA and LCA. Based on the experimental data, the pore tortuosity factor τ of coal was gained through using Carniglia's calculation model. Furthermore, multi-fractal singularity spectrum and the generalized spectrum were presented to describe the inhomogeneous PSDs of coal. Finally, the evolution of pore structure and microfractures as well as the mechanism of gas outburst under the condition of mining were discussed.

2 Experiments

2.1 Experimental Samples

The collected coal samples were from 2# coal seam (high-gas coal seam) in Dongpang mine of Xingtai Mining Bureau in Dameng Village, Qiu County, Hebei Province, China. The geographical coordinates of Dongpang mine are 37° 18′ N and 114° 20′ E. The 2# coal seam with the average thickness of 4.18 m is stable and has simple geological structure and low sulfur content (average 0.42%). It is the topmost and workable coal seam in the coal-bearing strata. The absolute gas emission of the mine was calculated to be 49.79 m^3/min and the relative gas emission to be 7.62 m^3/t in July 2014. Based on the analysis of microlithotype classification, there are less durite, xylovitrite and fusain in the 2# coal seam. The whole layer of the coal seam exists duroclarite, in which the semi-bright coal is distributed in the all parts.

The maximum reflectance of vitrinite and maceral for the collected coal samples is shown in Table 1. The results show that the proportions of vitrinite, inertinite, semi-vitrinite and exinite are 59.8%, 24%, 8.2% and 7.9%, respectively. The R_{omax} of 2# coal seam is 0.758%. The inorganic components mainly are clay (2.5%), followed by iron sulfide (0.7%).

Samples were collected from No.20011 working face of 2# coal seam with the mining depth as -490~-520 m and were divided into two groups as

Table 1 The basic information of coal samples

Coal seam	Drilling	Coal thickness	R_{omax}	Organic constituents				Inorganic components			
				vitrinite	Semi-vitrinite	inertinite	exinite	clay	iron sulfide	carbonate	silicon oxide
2#	20,011	1.63	0.758	59.8	8.2	24	7.9	2.5	0.7	/	/

shown in Fig. 1. One group of coal samples was cut from the intact coal block which was roughly a cube with the particle size less than 1 cm. The other group of samples was the pulverized coal drilled from the working face. Each group was randomly divided into 6 specimens, including the intact coal samples (I-1 ~ I-6) and the pulverized coal samples (P-1 ~ P-6). As shown in Table 2, the particle size of the pulverized coal changes from less than 0.2 to 5 mm. The largest contents of particles in pulverized coal are 0.3–5 mm particles and its average proportion is 77.82%.

2.2 Experimental Schemes

MIP was carried out to observe the microstructure characteristics of coal samples. Some parameters such as total pore volume, porosity and bulk density were measured by AutoPore IV 9500 mercury injection instrument in the laboratory of Thermal Physics of Tsinghua University in China. The surface tension of mercury was 4.85×10^{-3} N/cm, and the wetting angle was 130.000°. Coal samples were heated to 110 ℃ in a vacuum oven for 4 h. Under the action of external forces, the vacuumed samples were used to measure mercury intrusion volume.

LNA was done by the ASAP2020 automatic in the Comprehensive Thermal Physics of Thermal Physics of Tsinghua University. In the LNA, the temperature was 77 K and the adsorption medium was nitrogen of purity 99.999%. As the relative pressure (P/P_0) increased from 0 to 1, the quantity of adsorbed liquid nitrogen can be measured. The instrument could determine BET specific surface area, BJH adsorption cumulative volume, etc. Carbon dioxide was regarded as adsorbent in the LCA. American ASAP2020 automatic was also used to carry out the experiment under the condition of 293 K temperature.

2.3 Experimental Results

2.3.1 Mercury Intrusion Porosimetry

According to the work of Cai et al. (2013), a combined pore classification is applied: Super-micropore ($d < 2$ nm), micropore (2 nm $< d <$ 10 nm), transition pore (10 nm $< d <$ 100 nm), mesopore (100 nm $< d <$ 1000 nm), macropore ($d > 1000$ nm) and microfracture ($d > 10000$ nm), where d is the pore

(a) Intact coal
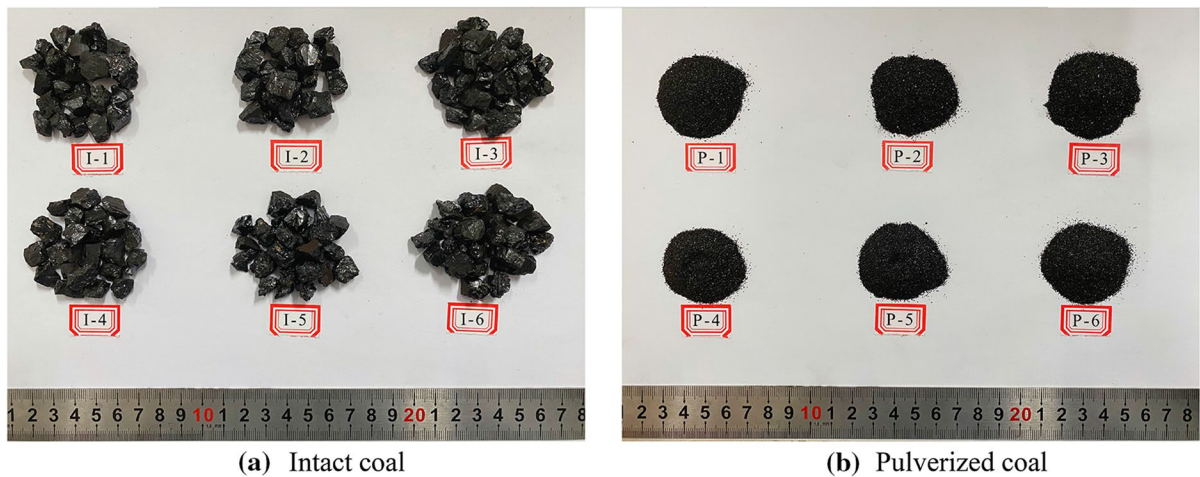
(b) Pulverized coal

Fig.1 The experimental samples of intact coal and pulverized coal

Table 2 Different size particle content of pulverized coal

Diameter of pulverized coal	~0.2 mm	0.2~0.3 mm	0.3~5 mm
The quality proportion (%)	16.14	6.05	77.82

size of coal. The MIP curves of the intact and pulverized coal samples are shown in Fig. 2.

The MIP curves of all samples are similar in shape, as shown in Fig. 2. The slopes of the curves at the initial phase increase sharply, indicating that there are a lot of macropores. With the increase of pressure, the curves tend to be flat, which means that mesopores and transition pores are less in the total pore volume. Because of the abundance of micropore contents, the slopes increase greatly again at the end of the curves. Comparing the hysteretic loops that is between the curves of mercury intrusion and extrusion, similar characteristics also can be observed. The narrow hysteretic loops suggest that semi-open pores are presented in coal samples, which influence the pore connectivity and is not conducive to gas desorption and migration.

2.3.2 Nitrogen and Carbon Dioxide Gas Adsorption

According to the liquid nitrogen adsorption experiment, the isothermal adsorption and desorption

curves of LNA testing are obtained as shown in Fig. 3.

Five types of hysteresis loops have been identified and correlated with different pore shapes such as: cylindrical shape, slit shape, wedge shape, ink bottle shape (Nie et al. 2015; Thommes et al. 2016). By observing Fig. 3, for all samples, adsorption and desorption curves are overlapped at a relatively low pressure, which demonstrates that a lot of closed and semi-closed pores exist in a small pore size range, for instance wedge-shaped and slit-shaped pore. When the relative pressure P/P_0 is about 0.5, the desorption curves of all the pulverized coal samples appear an inflection point of small drop, indicating that there are ink bottle shape pores. The high peak value of adsorption curve corresponds to the good adsorption capacity. Thus, the pulverized coal has the stronger adsorption capacity. Pore parameters of coal samples obtained by MIP and gas absorption are listed in Table 3.

Xu et al. (2010) pointed out that pore diameter decreased while the total volume of pores increased with the reduction of briquette particle size under the same geological conditions, and the pores were better developed and more evenly distributed. As we can see from Table 3, the average total pore volume and pore size of pulverized coal samples are 0.1098 mL/g and 16.03 nm, while that of intact coal samples are 0.0735 mL/g and 20.96 nm. The mean S_{BET} of the intact and pulverized coal is 0.627m²/g and 1.072 m²/g, respectively. It shows that compared to intact
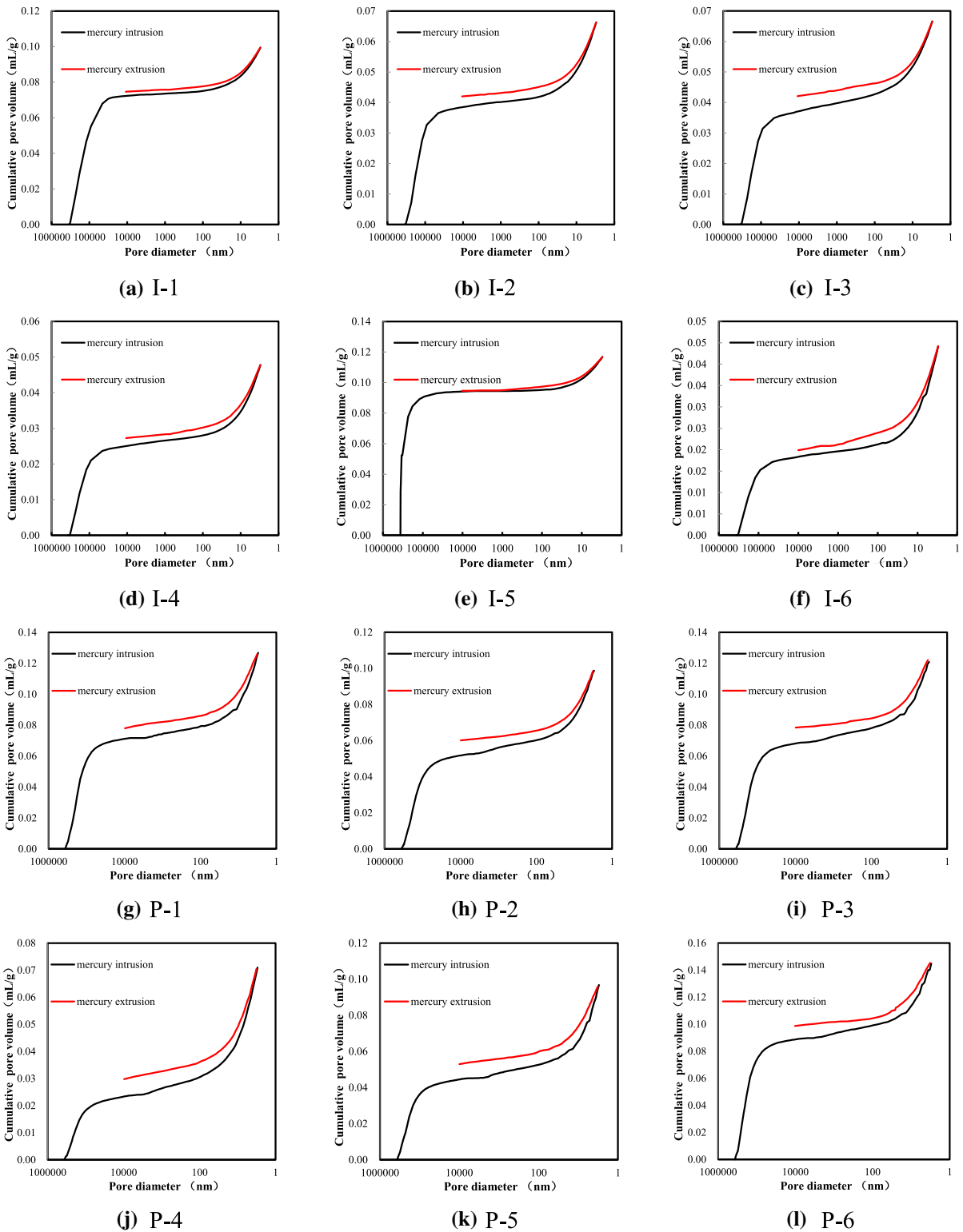
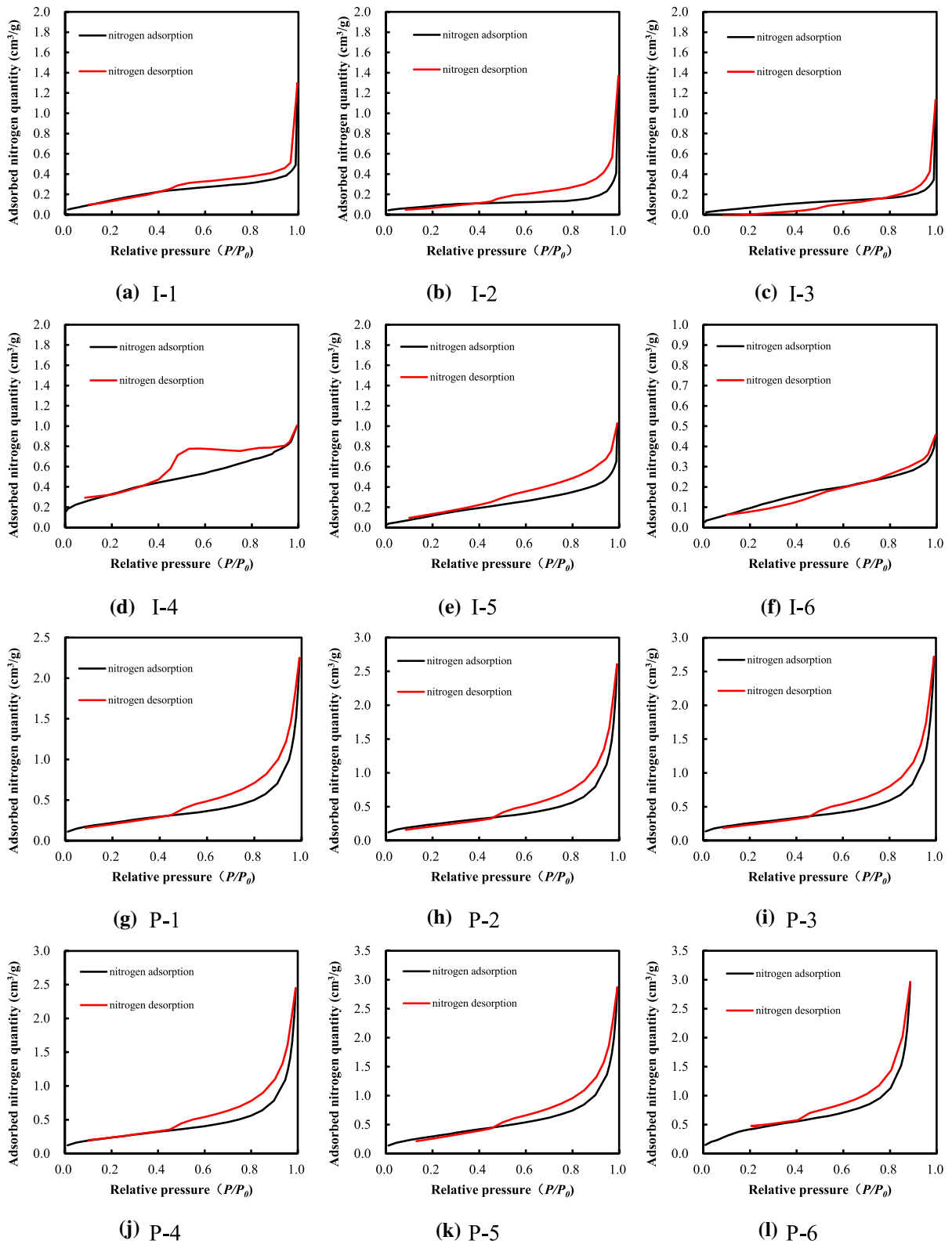**Fig.2** The mercury intrusion porosimetry curves of coal samples

Fig.3 Nitrogen adsorption and desorption curves of coal samples

Table 3 Parameters obtained from the above experiments

Sample ID	Parameters obtained from MIP					Parameters obtained from LNA		Parameters obtained from LCA	
	Total pore volume	Average pore diameter	Porosity	ρ_b	ρ_s	V_{BJH}	S_{BET}	Total pore volume	Total pore area
	(mL/g)	(nm)	(%)	(g/mL)	(g/mL)	(cm^3/g)	(m^2/g)	(cm^3/g)	(m^2/g)
I-1	0.0994	26.49	12.26	1.233	1.405	0.00079	0.686	0.0022	13.404
I-2	0.0663	17.87	8.52	1.286	1.405	0.00072	0.344	0.0049	24.094
I-3	0.0666	18.91	8.66	1.301	1.425	0.00057	0.326	0.0059	22.271
I-4	0.0478	15.64	6.67	1.395	1.495	0.00146	1.27	0.0049	20.308
I-5	0.1168	34.70	10.17	1.169	1.302	0.00104	0.64	0.0020	13.940
I-6	0.0442	12.16	5.68	1.285	1.362	0.00062	0.497	0.0019	12.242
Average	0.0735	20.96	8.66	1.278	1.399	0.00087	0.627	0.0036	17.710
P-1	0.1267	16.40	15.24	1.204	1.419	0.0035	0.832	0.0080	47.727
P-2	0.0988	16.70	12.07	1.222	1.389	0.00405	0.896	0.0088	50.078
P-3	0.1208	18.50	14.73	1.22	1.43	0.00418	0.937	0.0038	25.927
P-4	0.0710	11.30	9.03	1.271	1.397	0.00381	0.894	0.0044	29.909
P-5	0.0968	13.40	11.90	1.23	1.396	0.00443	1.172	0.0041	29.176
P-6	0.1448	19.90	16.88	1.166	1.402	0.00449	1.698	0.0061	37.498
Average	0.1098	16.03	13.31	1.219	1.406	0.00408	1.072	0.0059	36.719

ρ_b is the bulk density; ρ_s is the skeletal density; V_{BJH} is the BJH adsorption cumulative volume of pores; S_{BET} is Brunauer–Emmett–Teller specific surface area

coal, the cumulative pore volume of pulverized coal is greater and its pore structure is more developed.

3 Pore Structure Characteristic of Coal

3.1 Mercury Porosimetry Corrected

When the pressure is greater than a limit value, the measured increment of mercury volume is not entirely caused by the filling of mercury but by the compressibility of the coal matrix (Li et al. 1999). The pore volume increment ΔV_{obs} observed from MIP is expressed as follows:

$$\Delta V_{obs} = \Delta V_C + \Delta V_P \tag{1}$$

where ΔV_C is the volume increment produced by the compressive coal matrix, and ΔV_P is the actual pore volume increment of samples.

The combined analyses of MIP, LNA and LCA were applied to gain the comprehensive pore characterics. Without considering the compressibility of mercury, the compressibility coefficient K_C of coal matrix can be defined as:

$$K_C = \frac{dV_C}{V_C dP} \tag{2}$$

where dV_C/dP is the function of the change of coal matrix volume with pressure, and V_C is the corrected cumulative pore volume of samples.

As shown in Fig. 4, when the mercury intrusion pressure is greater than 20 MPa, the cumulative mercury intrusion volume and pressure of coal samples can be fitted into a good linear trendline, and all the R^2 are greater than 0.98. The same phenomenon can be found in Li et al. (2015).

Therefore, when the mercury intrusion pressure is greater than 20 MPa, $\Delta V_C/\Delta P$ can be expressed as:
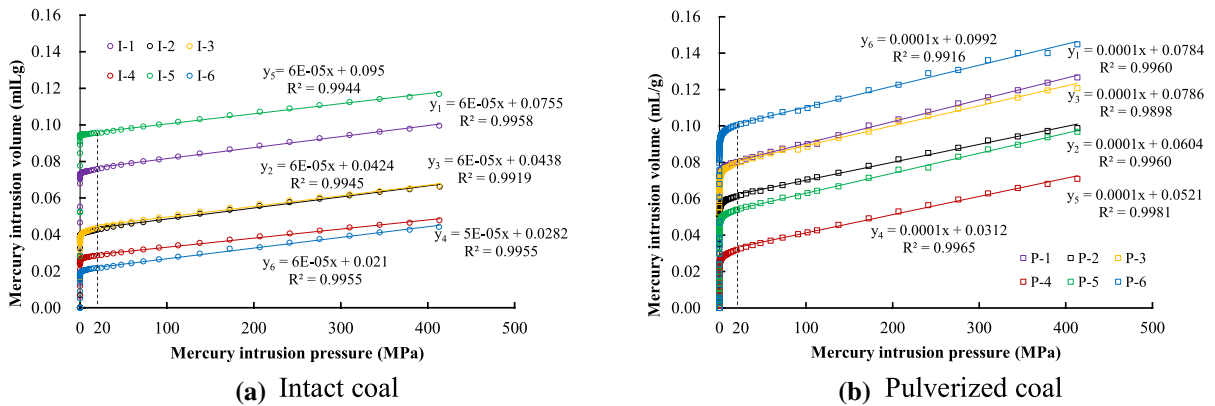
(a) Intact coal

(b) Pulverized coal

Fig.4 Linear regression of mercury pore volume versus pressure with pressure greater than 20 MPa based on MIP data

$$\frac{\Delta V_C}{\Delta P} = \beta - \frac{\sum\limits_{3nm}^{50nm} \Delta V_P}{\Delta P} \qquad (3)$$

where constant β represents $\Delta V_{obs}/\Delta P$ which is the slope of the trend line mentioned above, and the sum of the pore volume with pore size of 3–50 nm (the corresponding mercury intrusion pressure varies from 413 to 20 MPa) can be obtained from LNA.

Assuming $\Delta V_C/\Delta P$ is independent of the pressure, the K_C of 12 coal samples can be obtained from Eq. (2) by substituting dV_C/dP with $\Delta V_C/\Delta P$:

$$K_C = (\beta - \frac{\sum\limits_{3nm}^{50nm} \Delta V_P}{\Delta P})/V_C \qquad (4)$$

Combined with the pore volume got from LCA data (pore size less than 1 nm), LNA data (pore size of 1–3 nm), the corrected MIP data (pores size greater 3 nm), the real pore volume V_C and the compressibility coefficient K_C can be calculated, as shown in Table 4. Figure 5 shows the comparison of accumulative mercury volume before and after correction of coal matrix compression.

As shown in Table 4, the average compressibility coefficient of intact coal samples is

Table 4 Correction of the experimental data

| Sample ID	$K_C \times 10^{-3}$ (MPa^{-1})	Cumulative pore volume (mL/g)	Corrected cumulative pore volume V_C (mL/g)	R^2
I-1	0.754	0.1019	0.0788	0.9958
I-2	1.227	0.0713	0.0484	0.9945
I-3	1.185	0.0726	0.0504	0.9919
I-4	1.415	0.0530	0.0343	0.9955
I-5	0.854	0.1189	0.0975	0.9944
I-6	2.389	0.0463	0.0249	0.9955
Average	1.304	0.0773	0.0557	0.9946
P-1	1.022	0.1349	0.0966	0.9960
P-2	1.197	0.1078	0.0740	0.9960
P-3	1.098	0.1248	0.0897	0.9898
P-4	2.613	0.0755	0.0375	0.9965
P-5	1.502	0.1011	0.0653	0.9981
P-6	0.761	0.1511	0.1188	0.9916
Average	1.366	0.1159	0.0803	0.9946
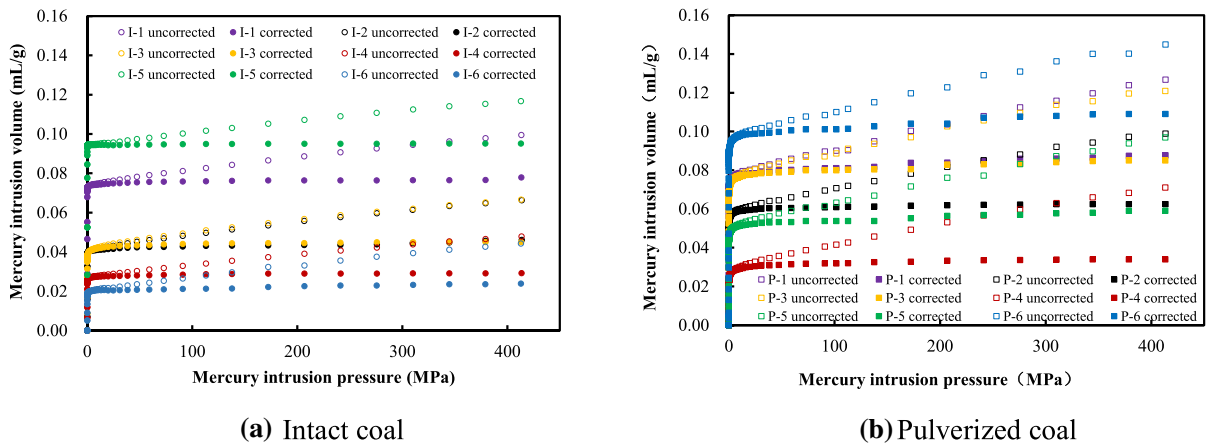
Fig.5 The cumulative mercury intrusion volume before and after correction

1.304×10^{-3} MPa^{-1} and that of pulverized coal samples is 1.366×10^{-3} MPa^{-1}. There is not an obvious difference on the compressibility of coal matrix between the intact and pulverized at the same sampling site. The average cumulative pore volume of intact samples before correction is 0.0773 mL/g and becomes 0.0557 mL/g after correction, which is reduced by 27.9%, while that of pulverized coal changes from 0.1159 to 0.0803 mL/g, which decreases by 30.7%. Combined with Fig. 5, it concludes that it is necessary to correct the pore volume from MIP when we describe the pore characteristics of coal samples.

3.2 Pore Tortuosity

Pore tortuosity factor τ is an important parameter to describe the structure of seepage-pores and microfractures. τ is defined as the ratio between the actual length L_0 of the seepage channel and the apparent length (macroscopic distance) L_t through the seepage medium. It is shown in the following formula (Khabbazi et al. 2016):

$$\tau = \frac{L_0}{L_t} \tag{5}$$

Carniglia (1986)has presented an equation to calculate τ, calling for physical performance data of porous materials obtained from Hg porosimetry. The equation could be expressed as follows:

$$\tau = x \cdot (0.92y)^{1+\varepsilon} \tag{6}$$

where x is a function of pore volume, y reflects the pore shape and is obtained from above experimental data, and ε is pore shape exponent ($\varepsilon = 1$ for cylinders). If $y < 1.1$, τ is equal to x. Where x and y can be expressed as:

$$x = 2.23 - 1.13 V_C \rho_b \tag{7}$$

$$y = \frac{2}{S} \sum \frac{\Delta V_i}{d_i} \tag{8}$$

where ρ_b is the bulk or particle density of the soild, S is the BET surface area, ΔV_i is the corrected increment of pore volume within the ith pore size interval I_i, and d_i is the average diameter within I_i. Based on Carnigila's equation, the author calculated the more accurate τ of coal samples by applying the corrected MIP data. The results of τ and the related parameters are listed in Table 5.

From the observation of Table 5, the average value of τ of intact coal samples is 2.316 while that of pulverized coal samples is 11.966. The greater the pore tortuosity, the greater the resistance through the porous medium and the lower the seepage pore connectivity, and therefore the lower the permeability (Chen et al. 2013). Thus, it can be deduced that the permeability and pore connectivity of pulverized coal is poor overall, which means that gas is easily accumulated in the area with the more pulverized coal.

Table 5 Pore tortuosity factor and the related parameters

| Sample ID	S_{BET} (m^2/g)	V_C (cm^3/g)	ρ_b (g/mL)	y	x	τ
I-1	0.686	0.0788	1.233	0.670	2.120	2.120
I-2	0.344	0.0484	1.286	1.146	2.160	2.403
I-3	0.326	0.0504	1.301	1.054	2.156	2.156
I-4	1.270	0.0343	1.395	0.442	2.176	2.176
I-5	0.640	0.0975	1.169	0.347	2.101	2.101
I-6	0.497	0.0249	1.285	1.259	2.194	2.941
Average	0.627	0.0557	1.278	0.820	2.151	2.316
P-1	0.832	0.0966	1.204	3.590	2.099	22.896
P-2	0.896	0.0740	1.222	1.684	2.128	5.110
P-3	0.937	0.0897	1.220	2.619	2.106	12.231
P-4	0.894	0.0375	1.271	0.784	2.176	2.176
P-5	1.172	0.0653	1.230	2.753	2.139	13.726
P-6	1.698	0.1188	1.166	2.987	2.073	15.657
Average	1.072	0.0803	1.219	2.403	2.120	11.966
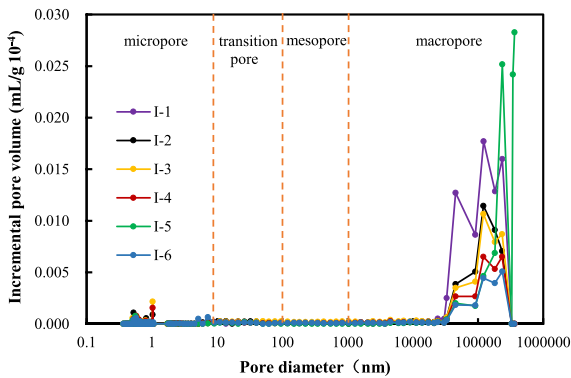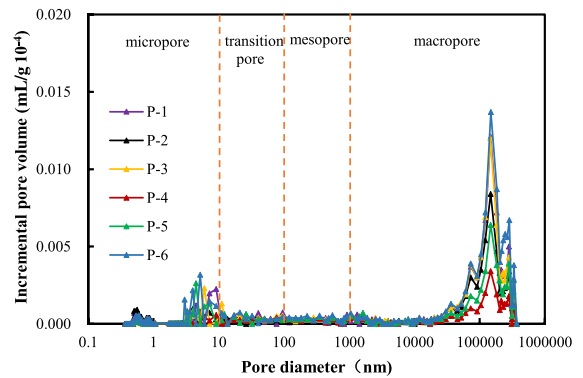
(a)   The intact coal samples   (b)   The pulverized coal samples

Fig.6 Pore size distributions of different coal samples

Fig.7 Pore volume of different pore size
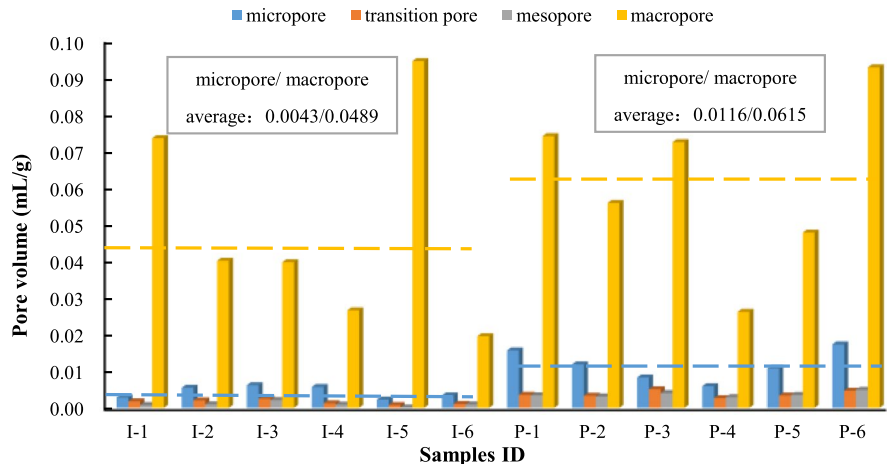
3.3 Pore size Distributions

Based on the corrected MIP data, the PSDs with different pore diameters are shown in Fig. 6 and the contents of different pores are drawn in Fig. 7.

As can be seen from Fig. 6, there are some differences in the PSDs when comparing with the intact and pulverized coal samples. For macropore with a pore diameter greater than 10 μm, the average pore volume of the intact coal is significantly more than pulverized coal. When the pores size is between 3.3 nm to 13.7 nm, pore volume of the pulverized coal is greater than the intact coal. Combined with Fig. 7, the average macropore volume of intact coal and pulverized coal are 0.0489 mL/g and 0.0615 mL/g, respectively. The average micropore volume of pulverized coal is 2.67 times that of intact coal. It can be concluded that the intact coal is dominated by macropores, while the main pore types of pulverized coal are micropores and macropores. It is commonly accepted that the micropores mainly control the gas adsorption and storage in coal, which also demonstrates that the pulverized coal has a strong adsorption capacity and gas accumulation more easily occurs in the more pulverized coal area.

4 Discussion and Analysis

4.1 Multi-Fractal Analysis

In order to calculate the multi-fractal singularity spectrum, three important parameters should be calculated: the probability quality distribution $P_i(\varepsilon)$, the singular exponent α and the dimension function $f(\alpha)$ (Caniego et al. 2003).The multi-fractal singular spectrum is a unimodal convex function. In previous studies, α and $f(\alpha)$ can be calculated as follows (Zhu et al. 2019):

$$\alpha(q) \propto \frac{\sum_{i=1}^{N(\varepsilon)} \omega_i(q,\varepsilon) \lg[P_i(\varepsilon)]}{\lg(\varepsilon)} \quad (9)$$

$$f[\alpha(q)] \propto \frac{\sum_{i=1}^{N(\varepsilon)} \omega_i(q,\varepsilon) \lg[\omega_i(q,\varepsilon)]}{\lg(\varepsilon)} \quad (10)$$

The generalized fractal dimension $(q \sim D_q)$ also can be used to study the pore characteristics. The multi-fractal generalized spectrum is a monotonically decreasing function. When $q \neq 1$, the generalized multi-fractal dimension D_q defined by Chhabra et al. (1989)is:

$$D_q = \frac{1}{q-1} \lim_{\varepsilon \to 0} \frac{\log \sum_{i=1}^{N(\varepsilon)} P_i(\varepsilon)^q}{\lg(\varepsilon)} \quad (11)$$

When $q = 1$, according to L'Hospital rule, D_1 can be calculated by $f(\alpha_{(1)})$ (Halsey et al. 1987; Chhabra et al. 1989):

$$D_1 = f'[\alpha(q)] = \lim_{\varepsilon \to 0} \frac{\sum_{i=1}^{N(\varepsilon)} \omega_i(q,\varepsilon) \lg[\omega_i(q,\varepsilon)]}{\lg(\varepsilon)} \quad (12)$$

Capacity dimension D_0, information dimension D_1 and correlation dimension D_2 can be obtained by the above formula (Martínez et al. 2010). D_0 represents the proportion of non-empty boxes containing some porosity in a contiguous small area; D_1 provides information about the concentrated distribution of porosity. At the same time, we also can get the Hurst index (Martínez et al. 2010):

$$H = (D_2 + 1)/2 \quad (13)$$

The related parameters are calculated as shown in Table 6 as well as the multi-fractal singular spectrum and the multi-fractal generalized spectrum are drawn in Fig. 8 and Fig.9, respectively.

The multi-fractal singularity index α_0 can represent the concentration of porosity in coal samples. The higher the value of α_0, the more apparent the fluctuation of the PSDs and the more inhomogeneous distribution of the porosity in a narrow range of pore sizes (Caniego et al. 2003). From the Table 6, the average value α_0 of intact coal is 2.887 and that of pulverized coal is 2.224, indicating that the porosity of intact coal is more densely distributed in a certain interval and the fluctuations of its PSDs are more obvious. The heterogeneous PSDs are also positive correlated with the width of multi-fractal singular spectrum $f(\alpha)$ or the values of $\alpha_{q-}\alpha_{q+}$ (Li et al. 2015). According to Fig. 8, the width of $f(\alpha)$ for intact coal (Fig. 8a) is wider than pulverized coal (Fig. 8b) overall, which also suggests that the PSDs of intact coal are more complex than pulverized coal.

Table 6 The calculated parameters of multi-fractal dimension

Sample ID	Parameters of multi-fractal singular dimension						Parameters of multi-fractal generalized dimension						
	α_0	α_{q+}	α_{q-}	$\alpha_0 - \alpha_{q+}$	$\alpha_q - \alpha_0$	$\alpha_q - \alpha_{q+}$	H	D_0	D_1	D_2	$D_0 - D_{10}$	$D_{-10} - D_0$	$D_{-10} - D_{10}$
I-1	2.966	0.671	5.010	2.295	2.044	4.339	0.898	1.725	0.928	0.796	1.019	2.919	3.937
I-2	2.640	0.605	4.758	2.036	2.117	4.153	0.905	1.725	1.014	0.809	1.070	2.679	3.749
I-3	2.578	0.651	4.768	1.927	2.190	4.117	0.931	1.725	1.095	0.862	1.027	2.694	3.721
I-4	2.565	0.671	4.579	1.894	2.015	3.908	0.919	1.725	1.054	0.837	1.024	2.516	3.540
I-5	4.034	0.266	6.134	3.768	2.100	5.868	0.715	1.725	0.596	0.430	1.429	3.966	5.395
I-6	2.538	0.687	4.470	1.851	1.932	3.783	0.949	1.725	1.130	0.898	0.996	2.428	3.424
Average	2.887	0.592	4.953	2.295	2.066	4.361	0.886	1.725	0.969	0.772	1.094	2.867	3.961
P-1	2.395	0.821	5.075	1.575	2.679	4.254	1.034	1.725	1.277	1.067	0.859	2.954	3.813
P-2	2.140	0.846	3.911	1.294	1.771	3.065	1.055	1.724	1.328	1.111	0.823	1.859	2.683
P-3	2.235	0.831	5.061	1.403	2.826	4.229	1.043	1.725	1.302	1.086	0.844	2.904	3.748
P-4	2.084	0.808	4.635	1.277	2.550	3.827	1.089	1.725	1.412	1.178	0.843	2.517	3.360
P-5	2.216	0.792	4.910	1.424	2.694	4.118	1.060	1.725	1.343	1.121	0.865	2.783	3.648
P-6	2.275	0.706	5.185	1.570	2.910	4.480	1.015	1.726	1.270	1.031	0.953	3.016	3.969
Average	2.224	0.801	4.796	1.424	2.572	3.995	1.049	1.725	1.322	1.099	0.865	2.672	3.537

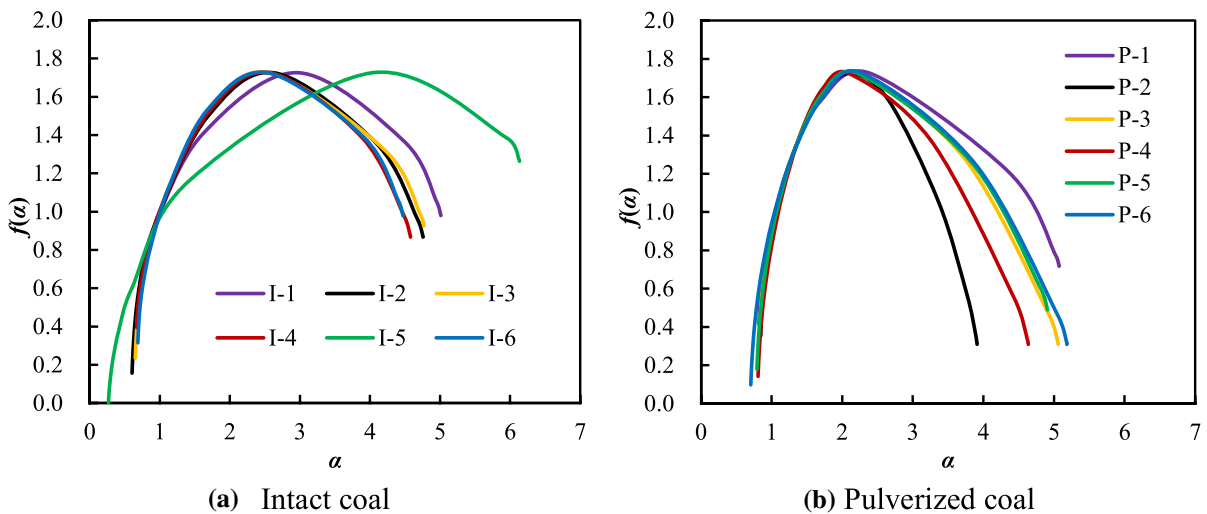

(a) Intact coal   **(b)** Pulverized coal

Fig.8 Multi-fractal singular spectrum of coal samples

Similarly, in the multi-fractal generalized spectrum, the value of D_1 and the width of D_q spectrum also can indicates the information of the heterogeneous PSDs. The further the value of D_1 goes away from D_0 or the wider the width of D_q, the more clustered the pores within a small pore size rang (Ferreiro and Vázquez 2010). Combined Table 6 and Fig. 9, the average value of D_1 for pulverized coal is 1.322, rather close to the average D_0 (1.725), and its width of D_q spectrum is narrower compared to the intact coal on the whole, indicating the low heterogeneity of the PSDs for pulverized coal. Meanwhile, the lower values D_1 and the wider the width of D_q spectrum of intact coal samples show that porosity concentrates across the range of pore sizes and its PSDs are more complex.

As we can see from the Fig. 8, α_0 divides the graph into two parts: the left region ((high value information, densely pore region) and the right region (low value information, sparse pore region). When the
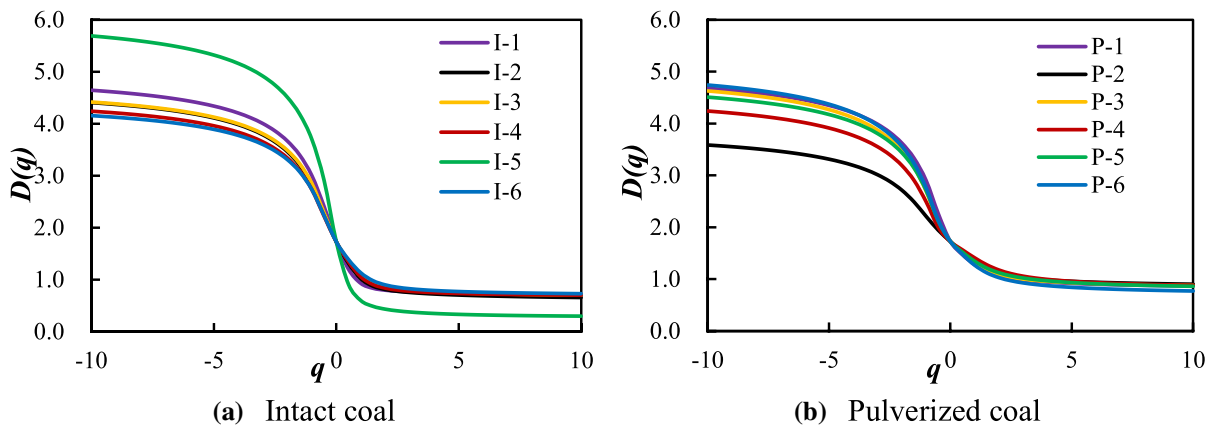
Fig.9 Multi-fractal generalized spectrum of coal samples

right is wider than the left ($\alpha_{q-}\alpha_0 > \alpha_0-\alpha_{q+}$), the PSDs are mainly controlled by the low value information. Conversely, it is dominated by high value information (Caniego et al. 2003). In Table 6, for the pulverized coal samples, the average value of $\alpha_{q-}\alpha_0$ (2.572) is greater than $\alpha_0-\alpha_{q+}$ (1.424), representing that the pores with small pore size play a dominant role in the PSDs of pulverized coal samples. On the contrary, the average value of $\alpha_{q-}\alpha_0$ (2.066) is smaller than $\alpha_0-\alpha_{q+}$ (2.295) for intact coal samples, which means that the PSDs of the intact coal are mainly controlled by large pores.

The Hirst index H is an important parameter to study the internal pore connectivity of coal and usually associates with the autocorrelation of the PSDs. When H is close to 1, the PSDs has a strong autocorrelation and the pore connectivity among different pore size intervals becomes better (Martínez et al. 2010). As we can see in the Table 6, the mean value of H of the intact coal is 0.886 while that of pulverized coal is 1.049. Since the dominance of the PSDs of pulverized coal is small pores while that of intact coal is large pores, the small pore distributions of pulverized coal exist the stronger autocorrelation and the better pore connectivity.

4.2 The Influence of Microfractures

There are a lot of microfractures in coal seam, which are the important channels for gas desorption and diffusion. As the mining depth increasing, the stress in overlying strata increases. The microfractures are affected by the overlying loading firstly,

followed by the macropores, mesopores, transition pores and micropores. The larger the loading is, the more pores are affected (Sun et al. 2020). Considering that the stress of coal samples in the laboratory has been relieved, the multi-fractal analyses are also carried out for the pore evolution without the effects of microfractures (pores size greater than 10 μm) in order to understand the pore structure of coal in deep coal seam. The multifractal parameters without the influence of microfractures are calculated as shown in Table 7.

From Table 7, the average value of $D_{-10} - D_{10}$ of pulverized and intact coal are 2.530, 2.157 respectively. When the stress is relieved, the effects of microfracture causes the average value of $D_{-10} - D_{10}$ of pulverized and intact coal increase to 3.537 and 3.961, as shown in Table 6. It shows that the microfractures lead to the higher fluctuation and greater complexity of the PSDs for all the samples. In addition, the variations on the value of $D_{-10} - D_{10}$ of intact coal are greater than that of pulverized coal, which indicates that the PSDs of intact coal are more homogenous when the influence of microfractures are not considered. The similar conclusion of coal samples can also be got by analyzing the multi-fractal singular spectrum.

Taking samples I-4 and P-4 for example, the multifractal singular spectrums whether considering the effect of microfractures were drawn in Fig. 10. It is obvious that without the microfractures, the width of $f(\alpha)$ decreases for samples I-4 and P-4, indicating that the evolution of microfractures make the complex and heterogeneous PSDs. Most of the microfractures

Table 7 Parameters of multi-fractal dimension without microfractures

Sample ID	Parameters of multi-fractal singular dimension						Parameters of multi-fractal generalized dimension						
	α_0	α_{q+}	α_{q-}	$\alpha_0 - \alpha_{q+}$	$\alpha_q - \alpha_0$	$\alpha_q - \alpha_{q+}$	H	D_0	D_1	D_2	$D_0 - D_{10}$	$D_{-10} - D_0$	$D_{-10} - D_{10}$
I-1	1.948	1.128	3.178	0.821	1.230	2.050	1.130	1.475	1.296	1.261	0.308	1.504	1.812
I-2	2.206	1.136	4.123	1.070	1.917	2.987	1.138	1.475	1.304	1.277	0.295	2.361	2.656
I-3	1.955	1.160	3.396	0.795	1.441	2.236	1.159	1.475	1.333	1.318	0.240	1.700	1.940
I-4	1.838	1.048	3.166	0.790	1.328	2.118	1.157	1.475	1.344	1.314	0.324	1.489	1.813
I-5	2.648	0.806	3.604	1.841	0.957	2.798	0.987	1.475	1.033	0.975	0.614	1.913	2.528
I-6	1.967	0.744	3.211	1.223	1.244	2.467	1.064	1.475	1.253	1.128	0.659	1.534	2.194
Average	2.094	1.004	3.446	1.090	1.353	2.443	1.106	1.475	1.261	1.212	0.407	1.750	2.157
P-1	2.131	0.789	3.726	1.342	1.595	2.937	1.053	1.479	1.222	1.106	0.621	2.004	2.625
P-2	1.857	1.012	3.629	0.845	1.772	2.617	1.149	1.479	1.351	1.298	0.386	1.900	2.286
P-3	1.913	0.779	3.735	1.134	1.822	2.956	1.095	1.479	1.303	1.190	0.611	1.996	2.607
P-4	1.913	0.922	3.493	0.991	1.580	2.571	1.134	1.475	1.321	1.267	0.455	1.783	2.239
P-5	2.044	0.703	3.710	1.341	1.666	3.007	1.052	1.479	1.242	1.104	0.695	1.984	2.679
P-6	2.007	0.779	3.850	1.227	1.843	3.071	1.051	1.479	1.247	1.103	0.636	2.105	2.741
Average	1.978	0.831	3.691	1.147	1.713	2.860	1.089	1.478	1.281	1.178	0.567	1.962	2.530

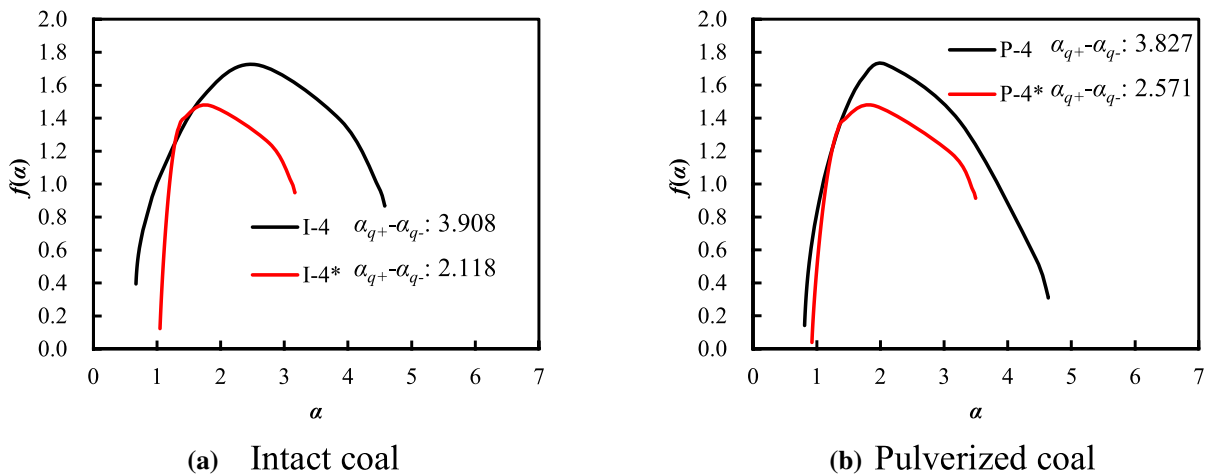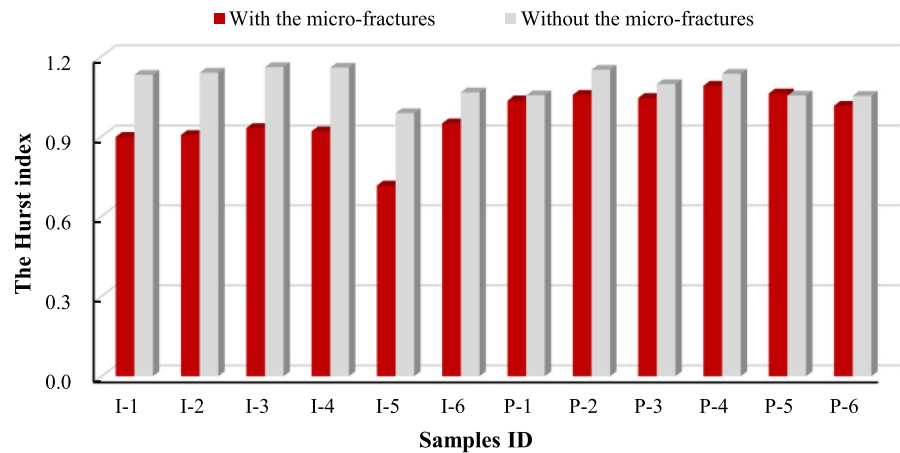**(a)** Intact coal   **(b)** Pulverized coal

Fig.10 Multi-fractal singular fractal dimension spectrum of I-4 and P-4

are compacted due to the stress in overlying strata, as well as the pore and microfracture distributions must change with the increase of the depth of the strata. Thus, under the condition of the real coal seam, the PSDs might be between the two states above mentioned.

The Hurst index H of all samples are plotted in Fig. 11. Without the effect of microfractures, the average values of H for intact and pulverized coal sample are 1.106 and 1.089, respectively. The

evolution of microfractures reduces the average H of the intact and pulverized coal to 0.886 and 1.049, respectively, which suggests that the microfractures have an obvious influence on H of intact coal and it results in the lower pore connectivity in the distributions of large pore.

The pore connectivity in the intact and pulverized coal is different, and the pore tortuosity of pulverized coal is greater but the permeability is lower. Thus, gas will be prone to adsorb and accumulate in the

Fig.11 The Hurst Index of coal sample

gularity index α_0 for the intact and pulverized coal samples are 2.887 and 2.224, respectively. The PSDs of intact coal are more complex and heterogeneous than pulverized coal. The average pore tortuosity τ of pulverized coal is 5.16 times that of intact coal, indicating that the pore connectivity of pulverized coal samples is worse on the whole.

5 Conclusions

The PSDs of the intact and pulverized coal samples, collected from the high gas mine in Hebei province, China, were analyzed by MIP, LNA and LCA. Multifractal characteristics of coal samples were presented based on the experimental data. The main conclusions are as follows:

(1) The compressibility of coal matrix has a significant influence on the pore volume in coal samples especially when the mercury pressure is greater than 20 MPa. Experimental results show that the contents of macropores are the most both in the intact or pulverized coal samples, but the average micropore volume for the pulverized coal samples is 2.67 times that of the intact coal samples. There is more likely to absorb gas in the pulverized coal area.

(2) The PSDs of coal samples have obvious multifractal characters. The average multi-fractal sin-

(3) During the process of mining, the vertical loading and horizontal unloading on coal seam ahead of mining face lead to the microfracture opening and propagation. The microfracture evolution makes the obvious change on the PSDs of intact coal. It indicates that mining causes gas desorption of the pulverized coal area but gas flow from pulverized coal area to the other area is not smooth. Gas might be prone to accumulate in the area with more pulverized coal.

Declarations

or kind in any product, service, and/or company that could be construed as influencing the position presented in, or the review of, the entitled manuscript.

References

Beamish BB, Crosdale PJ (1998) Instantaneous outbursts in underground coal mines: an overview and association with coal type. Int J Coal Geol 35:27–55. https://doi.org/10.1016/S0166-5162(97)00036-0

Cai Y, Liu D, Pan Z et al (2013) Pore structure and its impact on CH4 adsorption capacity and flow capability of bituminous and subbituminous coals from Northeast China. Fuel 103:258–268. https://doi.org/10.1016/j.fuel.2012.06.055

Caniego FJ, Martín MA, San José F (2003) Rényi dimensions of soil pore size distribution. Geoderma 112:205–216. https://doi.org/10.1016/S0016-7061(02)00307-5

Carniglia SC (1986) Construction of the tortuosity factor from porosimetry. J Catal 102:401–418. https://doi.org/10.1016/0021-9517(86)90176-4

Chen D, Pan Z, Liu J et al (2013) An improved relative permeability model for coal reservoirs. Int J Coal Geol 109–110:45–57. https://doi.org/10.1016/j.coal.2013.02.002

Cheng Y, Lei Y (2021) Causality between tectonic coal and coal and gas outbursts. J China Coal Soc 46:180–198. https://doi.org/10.13225/j.cnki.jccs.YG20.1539

Chhabra A, Meneveau C, Jensen R et al (1989) Direct determination of the f(α) singularity spectrum and its application to fully developed turbulence. Phys Rev A 40:5284–5294. https://doi.org/10.1103/physreva.40.5284

Ferreiro JP, Vázquez VE (2010) Multifractal analysis of Hg pore size distributions in soils with contrasting structural stability. Geoderma 160:64–73. https://doi.org/10.1016/j.geoderma.2009.11.019

Friesen W, Mikula R (1988) Mercury porosimetry of coals: pore volume distribution and compressibility. Fuel 67:1516–1520. https://doi.org/10.1016/0016-2361(88)90069-5

Fu XH, Qin Y, Xue XQ et al (2001) Research on fractals of pore and fracture-structure of coal reservoirs. J China Univ Min Technol (Engl Ed) 30: 225-228. https://doi.org/10.3321/j.issn:1000-1964.2001.03.003

Gauden PA, Terzyk AP, Rychlicki G (2001) New correlation between microporosity of strictly microporous activated carbons and fractal dimension on the basis of the Polanyi-Dubinin theory of adsorption. Carbon N Y 39:267–278. https://doi.org/10.1016/S0008-6223(00)00122-6

Giffin S, Littke R, Klaver J et al (2013) Application of BIB-SEM technology to characterize macropore morphology in coal. Int J Coal Geol 114:85–95. https://doi.org/10.1016/j.coal.2013.02.009

Guo J, Kang T, Kang J et al (2014) Effect of the lump size on methane desorption from anthracite. J Nat Gas Sci Eng 20:337–346. https://doi.org/10.1016/j.jngse.2014.07.019

Guo B, Li Y, Jiao F et al (2018) Experimental study on coal and gas outburst and the variation characteristics of gas pressure. Geomech Geophys Geo-Energy Geo-Resources 4:355–368. https://doi.org/10.1007/s40948-018-0092-8

Halsey TC, Jensen MH, Kadanoff LP et al (1987) Fractal measures and their singularities: the characterization of strange sets. Nuclear Phys B Proc Suppl 2:501–511. https://doi.org/10.1016/0920-5632(87)90036-3

Jin K, Cheng Y, Liu Q et al (2016) Experimental investigation of pore structure damage in pulverized coal: Implications for methane adsorption and diffusion characteristics. Energy Fuels 30:10383–10395. https://doi.org/10.1021/acs.energyfuels.6b02530

Karacan CO, Okandan E (2001) Adsorption and gas transport in coal microstructure: investigation and evaluation by quantitative X-ray CT imaging. Fuel 80:509–520. https://doi.org/10.1016/S0016-2361(00)00112-5

Khabbazi AE, Hinebaugh J, Bazylak A (2016) Determining the impact of rectangular grain aspect ratio on tortuosity–porosity correlations of two-dimensional stochastically generated porous media. Sci Bull 61:601–611. https://doi.org/10.1007/s11434-016-1020-3

Li YH, Lu GQ, Rudolph V (1999) Compressibility and fractal dimension of fine coal particles in relation to pore structure characterization using mercury porosimetry. Part Part Syst Charact 16:25–31. https://doi.org/10.1002/(SICI)1521-4117(199905)16:1%3c25::AID-PPSC25%3e3.0.CO;2-T

Li H, Ogawa Y, Shimada S (2003) Mechanism of methane flow through sheared coals and its role on methane recovery. Fuel 82:1271–1279. https://doi.org/10.1016/S0016-2361(03)00020-6

Li W, Liu H, Song X (2015) Multifractal analysis of Hg pore size distributions of tectonically deformed coals. Int J Coal Geol 144–145:138–152. https://doi.org/10.1016/j.coal.2015.04.011

Mandelbrot BB (1967) How long is the coast of Britain? Statistical self-similarity and fractional dimension. Science 156(3775):636–638. https://doi.org/10.1126/science.156.3775.636

Martínez FSJ, Martín MA, Caniego FJ et al (2010) Multifractal analysis of discretized X-ray CT images for the characterization of soil macropore structures. Geoderma 156:32–42. https://doi.org/10.1016/j.geoderma.2010.01.004

Muller J, McCauley JL (1992) Implication of fractal geometry for fluid flow properties of sedimentary rocks. Transp Porous Media 8:133–147. https://doi.org/10.1007/BF00617114

Nie B, Liu X, Yang L et al (2015) Pore structure characterization of different rank coals using gas adsorption and scanning electron microscopy. Fuel 158:908–917. https://doi.org/10.1016/j.fuel.2015.06.050

Suggate RP, Dickinson WW (2004) Carbon NMR of coals: the effects of coal type and rank. Int J Coal Geol 57:1–22. https://doi.org/10.1016/S0166-5162(03)00116-2

Sun B, Yang Q, Zhu J et al (2020) Pore size distributions and pore multifractal characteristics of medium and low-rank coals. Sci Rep 10:1–12. https://doi.org/10.1038/s41598-020-79338-3

Thommes M (2016) Physisorption of gases, with special reference to the evaluation of surface area and pore size distribution (IUPAC Technical Report). Pure and Applied Chemistry 87:25-25. https://doi.org/10.1515/ci-2016-0119

Wang Z, Cheng Y, Qi Y et al (2019) Experimental study of pore structure and fractal characteristics of pulverized

intact coal and tectonic coal by low temperature nitrogen adsorption. Powder Technol 350:15–25. https://doi.org/10.1016/j.powtec.2019.03.030

Xu J, Liu D, Peng S et al (2010) Experimental research on influence of particle diameter on coal and gas outburst. Chinese J Rock Mech Eng 29:1231–1237. https://doi.org/CNKI:SUN:YSLX.0.2010-06-020

Zhu J, He F, Zhang Y et al (2019) Fractal analysis in pore size distributions of different bituminous coals. Sci Rep 9:1–12. https://doi.org/10.1038/s41598-019-54749-z

Zhuo Q, Liu W, Xu H et al (2020) Effect of particle size distribution on filter cake pore structure and coal slurry dewatering process. Int J Coal Prep Util 00:1–16. https://doi.org/10.1080/19392699.2020.1781830